Research Square

Preprints are preliminary reports that have not undergone peer review.
They should not be considered conclusive, used to inform clinical practice,
or referenced by the media as validated information.

HTS-guided discovery of a novel plant-derived compound with retinal protective activity

A Bouaziz
Sorbonne Université, INSERM, CNRS, Institut de la Vision
G Puel
Sorbonne Université, INSERM, CNRS, Institut de la Vision
E Clérin
Sorbonne Université, INSERM, CNRS, Institut de la Vision
F Blond
Sorbonne Université, INSERM, CNRS, Institut de la Vision
I Harichane
Sorbonne Université, INSERM, CNRS, Institut de la Vision
M Cordonnier
Sorbonne Université, INSERM, CNRS, Institut de la Vision
V Forster
Sorbonne Université, INSERM, CNRS, Institut de la Vision
JA Sahel
University of Pittsburgh
S Picaud
Sorbonne Université, INSERM, CNRS, Institut de la Vision
E Genty
Laboratoires Greenpharma
B Francois
Laboratoires Greenpharma
P Bernard
Laboratoires Greenpharma
F Himbert
Laboratoires Greenpharma
I Audo
Sorbonne Université, INSERM, CNRS, Institut de la Vision
C Zeitz
Sorbonne Université, INSERM, CNRS, Institut de la Vision
T Léveillard
Sorbonne Université, INSERM, CNRS, Institut de la Vision

T Cronin

therese.cronin@inserm.fr

Sorbonne Université, INSERM, CNRS, Institut de la Vision

Research Article

Keywords:

Posted Date: November 11th, 2026

DOI: https://doi.org/10.21203/rs.3.rs-11688985/v1

License: This work is licensed under a Creative Commons Attribution 4.0 International License.
Read Full License

Additional Declarations: Competing interest reported. The compound described here is the subject of a patent issued to the authors in 2023: WO2023139091A1

HTS-guided discovery of a novel plant-derived compound with retinal protective activity

Authors: Bouaziz A[1]*, Puel G[1]*, Clérin E[1], Blond F[1], Harichane I[1], Cordonnier M[1], Forster V[1], Sahel JA[1, 2,3], Picaud S[1], Genty E[4], François B[4], Bernard P[4], Himbert F[4], Audo I[1, 3], Zeitz C[1], Léveillard T [1†], Cronin T[1]

***Co-first authors**

[†] Deceased. Thierry Léveillard passed away on the 07 June 2023

Affiliations

1 Sorbonne Université, INSERM, CNRS, Institut de la Vision, Paris, France.
2 Department of Ophthalmology, The University of Pittsburgh School of Medicine, Pittsburgh, Pennsylvania.
3 Centre Hospitalier National d'Ophtalmologie des Quinze-Vingts, Centre de Référence Maladies Rares REFERET and INSERM-DGOS CIC 1423, Paris, France.
4 Laboratoires Greenpharma, Orléans, France

INTRODUCTION

During the early modern age, investigations into the properties of different botanical species formed an integral part of medicine. Renaissance polymaths described the anti-inflammatory effects of plants, using crude extracts with multiple phytocompounds to treat infections[1,2]. Ocular medicine had one very early success story. The first formal text of ophthalmology, "Ten Treatises on the eye", written by the Arabic court physician, Hunain Ibn Ishâq in the tenth century, had already described the mydriatic ocular effects of the plant Atropa Belladonna[3]. By the 19th century, extracts of atropine purified from Atropa Belladonna led to what is today the most used drug in the eye-clinic[4]. However, apart from atropine and salves for the exterior of the eye, the historical record shows that ophthalmic uses of the new remedies coming from tropical plants were rare, perhaps due to the sensitivity of the corneal tissue and the high risk of corneal irritation from crude extracts of plants, and particularly tropical plants, and as such the field of ophthalmology never developed a strong natural-product tradition. There has been some correction over the last five decades with phytocompounds being newly tested in the treatment or prevention of glaucoma, macular degeneration and neuroinflammation. The most well-known is the vast clinical trial testing carotenoid-mediated antioxidant protection of photoreceptors in the AREDS2 formulation[5,6]. However, these efforts have had limited success as many of the known plant-derived molecules show low bioavailability in the retina, a major limitation for clinical translation[7]. Furthermore, the belief persists that the low-hanging fruit of therapeutic plant molecules, such as morphine, quinine and atropine, have long been discovered and what remains has lower potency and limited clinical returns.

We set out to determine whether this assumption is correct - at least as it applies in the field of ophthalmology. We were looking for phytocompounds that support the cone photoreceptor, the primary cell responsible for our visual acuity and our colour vision. This metabolically fragile retinal neuron relies heavily on substrates from neighbouring cells to support its function, leading us to hypothesize that equivalent secondary metabolites from plants may also offer a supportive role[8–12]. A high-throughput screen of secreted retinal compounds carried out 20 years ago on

pure chicken cone photoreceptor cultures led to the development and successful clinical translation of a neuroprotective factor termed Rod-derived Cone Viability Factor, RdCVF[13]. We employ the same approach here. We use as a bench-marking control, the berries of the plant *Lycium barbarum*, commonly called goji berries, which first appeared in Chinese pharmacopoiea 2300 years ago with extracts being used to treat a variety of ailments including those linked to vision [14]. These berry extracts also carry the components of the AREDS2 formula tested in a number of clinical trials for macular degeneration[5]. After an initial High Content Screen (HCS) of over 800 plant extracts on chicken cone culture, we selected Uvariae Chamae (*Uc*) as a promising source of pro-survival factors. This medicinal tropical plant was described within West African pharmacopoeias as having significant antimalarial activity due to antibiotic and anti-inflammatory compounds[15,16]. We followed up the initial screen with a second screen of 300 secondary metabolites from *Uc* to select one compound for further purification and characterization. The fragility of the cone photoreceptor comes from its high anabolic and catabolic requirements coupled with an extreme sensitivity to oxidative stress. We evaluated the final triaged *Uc* molecule within this context, focusing on the effects on changes in glycolysis and mitochondrial respiration in treated retinal tissue. We describe here the characterization of the molecule, its therapeutic potential and the potential that such phytochemical pipelines offer for treating degenerative retinal disease.

RESULTS

High content screening of medicinal plants for cone photoreceptor protection

Unlike the retina of mammals, the cone photoreceptors in bird species greatly outnumber rods, making their retinas useful in a screen for cone therapies[17]. We have adapted 96-well plates to culture retinal precursors from the retina of chicken embryos at this early stage of their development[18]. In these primary cultures, cones represent 80% of the cells after *in vitro* differentiation. In the absence of supportive compounds and of serum, the cells will degenerate over a period of one week[19] (Fig. 1A). To confirm the presence of cones, assess their morphology, and specifically monitor their degeneration, visinin staining was performed at specific time points during this 7-day period (Fig. 1B).

To establish an initial benchmark for cone survival from which to compare the efficacy of the phytocompounds, we tested different extracts from 200 selected plants that have known cyto-protective properties (Table S1). The berry Fructus barbarum, (*Fb*) has reported antioxidant properties and has, as its major constituents, carbohydrates, phytoestrogens, amino acids, vitamins and cartenoids[20,21]. The principal cartenoids, zeaxanthin and lutein, are also present in the human macula with a role in protection against light-induced retinal damage[22,23]. Having tested the concentrations of lutein and zeaxanthin in ethyl acetate extracts from *Fb* we found levels below 0.1 µg/ml for both. We therefore compared these purified pigment carotenoids at concentrations of 0.1 - 1 µg/ml with the whole extract of *Fb* and with resveratrol, a polyphenol compound shown to have antioxidant properties and a beneficial effect on retinal health[24–26]. While the purified compounds do not show a significant protective effect, the complete *Fb* extract shows a greater than 290% increase in cone number (Fig. 1C). This extract was subsequently used as a benchmark for efficacy in the HCS. The pipeline for the HCS involved initial extraction of bioactive extracts from the leaf, bark, grain and fruit of each of the 200 plants, giving

800 distinct extracts (Fig. 1D). This was followed by preparation of the cone-enriched cultures from developmental stage 29 chick retinas which were plated at two cell densities in 96-wells for tests against two concentrations of extracts, 10 and 100µg/ml before analysis of the cone viability factor (cone number test /cone number vehicle) [27]. The predefined plate layout (Fig. S1) and the full data from two hundred 96-well plates is presented in Mendeley repository (doi : 10.17632/2752kfkxf2.1). From this toxicity screen only 30 plants were selected for a second round of selection, which focused on leaf extracts at 100 µg/ml, and tested on 1 x 10^5 and 2 x 10^5 enriched cultures of chicken cone cells. A 3D representation of the cytoprotective effects versus cytotoxic effects were plotted in 3D (Fig. 1E) with the histogram amplitude representing the viability factor for each extract (see Methods section for more details). This narrowed down the search to one plant, Uvaria chamae (*Uc*) showing a viability factor of 7,57 at the higher cell density with ethyl acetate extraction. It was notable from phylogenetic analysis of all tested plant extracts, that the two most protective plants – *Annona Senegalensis* (*) and *Uvaria Chamae* (**) are very closely related (Fig. S2). From this we infer that the secondary metabolites of these Annonacae plant families, having evolved for ecological defense, show potent and diverse bioactivities and may be a rich source of neuroprotective compounds.

Fractionation of Uvaria chamae extracts distils cone photoreceptor protective activity

Uvaria chamae (*Uc*), having the most beneficial effect on the chick cone culture, includes four distinct plant species. The four species (*Uc*a, *Uc*b, *Uc*c, *Uc*d) were tested for cone rescue based on cross-comparison of leaf extract concentration versus cell number. From this test *Uc*a species was selected for the highest overall cone protective effect at both selected concentrations in the chicken cone culture and was carried forward for fractionation and purification of the active compound (Fig. 2A). For the first fractionation, 100 kg of the leaves were dried, ground and filtered of residue and the crude fractions extracted on a reverse-phase HPLC column with increasing levels of methanol (Fig. 2B). From this first column, fraction *Uc*aC3 showed the most potent activity with a 118% increase in cone survival compared to vehicle (Fig. 2C). This fraction was increasingly purified over three further iterative fractionation and potency testing steps with a final iteration involving 8 sub-fractions with fraction 8 found to retain the biological protective activity of the first crude fraction, *Uc*aC3 with a 200% increase in cone survival (Fig. 2D and 2E). This fraction 8 was subsequently divided by a liquid-liquid HPLC to separate apolar, polar and alkaloid fractions. These fractions were again tested on the cone cultures identifying the alkaloid fraction as most likely to carry the cone survival factor (S3). Fractions containing purely active molecules were then isolated by reverse-phase HPLC over methanol with three distinct fractions separated and tested for potency (Fig. 2F). The third alkaloid-rich fraction, named *UcA*C3F8f3 was shown to clearly carry the active metabolite with a 4.5-fold increase in cone-survival at 0.1 µg/ml rising to 6-fold at 10 µg/ml (Fig. 2G). Furthermore, a notable increase in cone neurite outgrowth was observed by calcein staining after a week of incubation with just 50 ng/ml of the final fraction *UcA*C3F8f3 (Fig. 2I).

Structure and related activity of the final Uvaria chamae neuroprotective compound from fraction *UcA*C3F8f3

The entire fractionation procedure as summarised in figure 2H, was repeated on a new batch of 100 kg of *Uc* leaves obtained from the same culture of the same season in Burkina Faso, to obtain the fraction used for isolation of secondary metabolites by mass spectrometry, from which it was determined that it contained 38 distinct chemical entities ranging in size from 328 to 1 284 Da (Fig. 3A).

Retention Time (mins)	m/z	Identified entities	Function
5.53	257	(S)-5,dihydroxyflavanone	Anti-microbial
	121	Benzene, 1-methoxy-2-{(phenylmethoxy)methyl}-o-Methoxybenzyl ether	Anti-tumoral
10.25	360	o-Anisyl benzoate	
10.96	281	3-phenyl-1-(2,4,6-trihydroxy-phenyl)-1-propanone	
12.08	323	Anguvetin	Anti-microbial, cytotoxic
12.76	323	1-(2,4-dihydroxy-6-methoxy-3,5-dimethylphenyl)-3-phenyl-1-propanone	Anti-tumoral
24.64	578	Diepolyrollin	Anti-tumoral
27.77	386	(S)-chamanetin, flavanoid	Anti-tumoral
31.35	507	Diuvaretin, flavanoid	Bactericide, antiseptic
33.59	325	Nornantenine, alkaloid	Cytotoxic
38.68	611	Tripoxyrollin, acetogenin	Anti-tumoral
39.75	627	Chamuvarinin, acetogenin	Anti-tumoral

Table 1: Twelve annotated compounds identified from the 38 species detected by mass spectrometry on a fresh preparation of UcAC3F8f3 fraction from Uvaria Chamae.

We identified 12 molecules from these entities with known structures and associated CAS identifiers (Table 1). These 12 molecules were classified according to their polarity and the presence of nitrogen-containing ring structures as is characteristic of the alkaloids often found in medicines. The final scaled-up compound was shown to retain the activity of the original product and the structure of the active metabolite was characterized by our industry collaborators, GreenPharma, giving a compound $C_{37}H_{66}O_7$ (Fig. 3B). This is strikingly similar to an acetogenin, a class of natural products from the Annonaceae plant family that often show neurotoxicity, likely due to inhibition of the NADH dehydrogenase flavoprotein of Complex I (CI) of the Electron Transport Chain (ETC)[28,29]. The *Uc* species is known to be rich in acetogenins as well as benzophenones, flavanoids and alkaloids[30]. The molecule has one notable feature distinguishing it from a classical acetogenin, having an open rather than closed terminal gamma-lactone ring (fig. 3B). As Acetogenins typically have negative effects on mitochondrial respiration, we considered whether the neuroprotection of cones by the final fraction *Uc*AC3F8f3-derived compound limits mitochondrial pyruvate-supported respiration, thereby boosting secondary anabolic metabolism through glycolysis. We tested the fraction *Uc*AC3F8f3 on Retinal Pigmented Epithelium (RPE) primary cells cultured from pig eyes (Fig. 3C). RPE was selected as these cells are highly reliant on mitochondrial respiration for survival and are the first cells to die in AMD [31–

[34]. The mitochondrial membrane potential is a reliable read-out of mitochondrial activity and was measured using the protonophore TMRM at concentrations of 50 nM. The TMRM-induced responses of RPE cells in explanted pig eye-cups were initially measured at the single-cell level by time-lapse imaging with the effects of the Complex V blocker oligomycin and the uncoupler FCCP used to reveal mitochondrial complex activity (Fig. 3D and S4). Having confirmed that TMRM can be used reliably to track mitochondrial bioenergetic profile, we tested the fluorescence responses to drugs in RPE cells pretreated with *UcAC3F8f3* using kinetic plate-reader measurements. Cells were exposed to varying concentrations of *UcAC3F8f3* overnight before TMRM analysis. Mitotracker was used to normalise the fluorescent readings by normalising for plasma membrane changes under the assumption that mitochondrial number was not impacted by *UcAC3F8f3*. We find that the compound hyperpolarizes the membrane only at very high concentrations (1 mg/ml) as compared to the depolarizing effect of Rotenone, a well-established CI inhibitor, though FCCP continues to depolarize even in the Rotenone condition (Fig 3E). The results suggest that RPE mitochondrial bioenergetics are not significantly impacted by overnight incubation with *Uc*AC3F8f3. Given the open gamma-lactone ring, *Uc*AC3F8f3 may have a reduced binding affinity and electrophillicity compared to typical acetogenins and thus show limited direct CI interaction. To further investigate any potential mitochondrial interaction, the cone cultures were treated with *Uc*AC3F8f3 in the presence of an inhibitor of mitochondrial pyruvate uptake, 2-cyano-3-(1-phenyl-1H-indol-3-yl)-2-propenoique (UK5099) (Fig. 3F). Blocking substrate uptake with 50ng/ml of UK5099 was not found to impact the protective effect of the purified fraction *UcAC3F8f3* suggesting that active mitochondrial respiration was not a target of the compound's neuroprotective activity (Fig. 3G).

The cytoprotective activity of the *Uc*AC3F8f3 depends on active glycolysis

While the structure of *Uc*AC3F8f3 led us to investigate mitochondrial activity in RPE, there is more evident inherent dependence of cone photoreceptors on aerobic glycolysis rather than oxidative phosphorylation for their viability. Glucose uptake, as the very first step of glycolysis has been described as the target for another cone protective product, RdCVF[13]. If the therapeutic effects of *Uc*AC3F8f3 is dependent on the activity of the glycolytic pathway then increased substrate for glycolysis may enhance the protective effect. When the concentration of glucose in the cone culture media was increased from 15 mM to 30 mM a moderate increase in protection was afforded by *Uc*AC3F8f3 (Fig. 4A). We could also validate directly that the cones did indeed have increased glucose uptake upon treatment with the compound by glucose uptake assay using plasmid-derived 2-NBDG (Fig. 4B). This suggests that increased glycolytic flux allowed for increased protection. As a counter to a glycolytic boost, we also tested how the treated cones respond to a metabolic glycolytic stress by treating the cone culture with oxamate, an analogue of pyruvate that inhibits the activity of lactate dehydrogenase (LDH) (Fig. 4C)[35]. We find that increasing concentrations of oxamate, from 12.5 to 25 nM, does indeed cause impact the effect of *Uc*AC3F8f3 from a 4-fold cytoprotection effect to no protective effect (Fig. 4D). The LDH step is downstream in the 10-step glycolysis pathway however its inhibition means that NAD+ cannot be regenerated during the pyruvate to lactate conversion. This creates a bottleneck in glycolytic flux upstream at the NAD+ dependant GAPDH step, stalling glycolysis. This suggests that the protection afforded by this compound is upstream of the GAPDH-catalytic step of glycolysis.

To determine where in the glycolytic pathway *Uc*AC3F8f3 exerts its activity we measured the different glycolytic metabolites that are present following four days of incubation of a chick cone culture with or without *Uc*AC3F8f3. From this we observe a significant reduction in glucose-6-phosphate (G6P) and frucose-6-phosphate (F6P) while all other metabolites downstream of F6P are not significantly changed (Fig. 5A). This suggests that *Uc*AC3F8f3 has the effect of accelerating glycolytic flux at the point of conversion of F6P to F16BP, a reaction catalyzed by phosphofructokinase (PFK). This reaction rate is in turn determined by the activation of another enzyme called 6-phosphofructo-2-kinase/fructose-2,6-bisphosphatase-2 (PFKFB2)[36]. PFKFB2 is a bifunctional enzyme that carries both a kinase and phosphatase domain ensuring that it can both produce and degrade fructose 2,6-bisphosphate (F26BP) depending on its own phosphorylation state[37]. When phosphorylated, PFKFB2 acts as a kinase and activates glycolysis though a boost of the enzyme phosphofructokinase (PFK), however unphosphorylated PFKFB2 converts F26BP back to F6P slowing down the rate of glycolysis. In this way PFKFB2 controls the cellular pool of F26BP, a potent allosteric regulator of glycolysis, thus making PFKFB2 a master regulator of glucose utilization in the cell[38]. We examined the level of PFKFB2 transcripts in chicken cone culture with increased glucose in the culture medium and after incubation with medium containing 10 ng/ml of *Uc*AC3F8f3 and find that expression is significantly induced under both conditions (Fig. 5B and 5C). We further examined the effects of overexpression of PFKFB2 on the protection afforded by *Uc*AC3F8f3. We found that electroporation of the chick retinas with mouse *Pfkfb2*-expressing plasmid before cone photoreceptor dissociation and culturing allowed for a modest increase in cone cell survival compared to *Uc*AC3F8f3 alone (Fig. 5D). *Uc*AC3F8f3 supports the cone photoreceptors in enriched cone culture by enabling the glycolytic flux towards anabolic ends with the bifunctional enzyme PFKFB2 as its direct or indirect target. This protective mechanism may be optimally isolated in an enriched cone culture with excess of glucose. However, ultimately the relevance of the compound for therapeutic translation depends on the capacity of *UcAC3F8f3* to preserve cones in a whole intact retina.

Testing the therapeutic potential of *Uc*AC3F8f3 on *rd1* mouse and pig retinal explants

Subretinal injection of the unprotected molecule *in vivo* is not feasible as the compound will be cleared from the subretinal space, an outcome that may be especially relevant in the degenerating retina where subretinal macrophage is abundant. We therefore started full tissue evaluation by testing the efficacy of the fractionated phytocompound on retinal explants from the most well-established animal model of retinal degeneration, the *rd1* mouse[39]. The retina of this mouse succumbs to severe photoreceptor degeneration from 1 week of age. To test the preservation of cones, retinas from mice (n = 13) at 21 days of age were dissected and cultured as explants for 1 week in the presence or absence of 1.5 µg total of *Uc*AC3F8f3. This high concentration was estimated as necessary for access to the full tissue compared to the pure cone culture tests and was in the range of concentrations tested for the original unfractionated UcA extract (Fig. 2A). The late stage of the *rd1* pathology was selected as there are no surviving rod photoreceptors left, and it is from this stage that the peak of cone death ensues. After 1 week of culturing the retinas were fixed and labelled for the presence of cone outer segments before counting on an automated cone-counting platform[40]. No difference in outer segment counts was found in this *ex vivo* model (Fig. 6A). However, the severity of degeneration in this model and in

this set-up may have prevented access to a therapeutic window and we therefore tested in an alternative model of retinal degeneration.

Pig retinas are closer anatomically to human eyes, not just in size but in the presence of a cone-rich area centralis. A similar *ex vivo* set-up was therefore tested with pig eyes (n = 6) dissected and explanted on which a cone-specific degeneration was induced. This cone atrophy is induced by a transport inhibitor (Forster *et al*, publication currently under review). The pig retina is cultured during seven days with the blocker leading to photoreceptor degeneration (termed "Transport blocker (RD)"). We assessed the ability of the *Uc*AC3F8f3 fraction to protect the retina in this model during the atrophy induction, by measurement of atrophy at the end of the 7-day period. Three regions of 2 mm^2 biopsies were scanned by confocal imaging and >80 µm hypofluorescent regions combined as well as holes in masked areas were counted in the z-projections for each region (Fig. 6B). This analysis showed the significant effect of the degenerative treatment on the explant ('Vehicle control' Fig 6E). While the absolute number of lesions was not significantly changed upon treatment with *Uc*AC3F8F3 (Fig 6C), the size of lesions was significantly reduced (Fig 6D and table 2).

Groups (n=6)	Lesions /field	Hypo	Holes	Total area	Hole area
Control	1.30	0.35	0.95	4.2%	3.5%
RD	2.08	0.77	1.31	7.4%	6.1%
10 ng *Uc*AC3F8f3	1.33	0.67	0.67	3.4%	2.4%
10 µg *Uc*AC3F8f3	1.22	0.83	0.39	3.0%	1.7%
100 µg *Uc*AC3F8f3	1.11	0.56	0.56	3.3%	2.4%

Table 2: Analysis of macroscopic lesions showing the average values from 3x FOV on each retinal explant from n=6 pigs. Lesion/field reflect the combination of hypo-fluorescent and hole-like lesions.

At all three concentrations a consistent protective effect on cone packing in all eyes, supported the potential of *Uc*AC3F8F3 to protect the retina during stress-induced degeneration as seen in representative images from the retinal flatmounts (Fig 6E).

DISCUSSION

In this work we have screened and fractionated neuroprotective secondary metabolites from 800 plant extracts to identify one compound from the fraction *UcAC3F8f3*, which we later termed 'Geralexin' that preserves photoreceptors in a chick cone culture. While this compound has an acetogenin-like structure, it has features that make it unique compared to known acetogenins. The protective effect may not depend on an interaction with complex I of the ETC, as is typical of classical acetogenins as this effect is essentially neurotoxic. Classical acetogenins competitively inhibit insertion of CoQ into the ubiquinone binding pocket preventing its reduction by complex I and thereby blocking electron transport and proton pumping by the ETC. The long hydrophobic tail of acetogenins, which mimics the isoprenoid tail of ubiquinone, is present in *Uc*ACa3F8f3 so it may still allow it to embed in the mitochondrial membrane near complex I[41–43]. However, the lactone head group of *Uc*AC3F8f3 is not closed and may not be capable of forming hydrogen bonds to interact with key residues of the CoQ pocket. *Uc*ACa3F8f3 would therefore not compete with CoQ for positioning in the pocket. Numerous studies have demonstrated that

photoreceptors rely more heavily on glycolysis rather than on mitochondrial-mediated respiration for immediate ATP production. Indeed, we find the principal biochemical change induced by the isolated compound is within the glycolytic pathway, which is the source of therapeutic targets for other cone-protective compounds and strategies that have been described[32,36,44]. We further identified PFKFB2 as a potential target of *Uc*ACa3F8f3 activity. While the mechanism is not yet clear, one possibility involves activation of the basic helix-loop-helix leucine zipper, MondoA. Upon sensing changes in mitochondrial membrane potential due to *UcAC3F8f3* insertion in the inner mitochondrial membrane (as demonstrated at higher concentrations in our TMRM study), this metabolic sensor may be released from its location on the mitochondrial outer membrane for translocation to the nucleus and activation of targets involved in glucose metabolism, including PFKFB2[41].

In typical rod-cone forms of retinal degeneration a bio-energetic crisis leads to cone death due to failure of the RPE to release glucose to cones, as such improving the efficiency of glycolysis may be of value[10,11]. Alternatively, in RDs such as AMD, where the cone pathophysiology derives from oxidative stress rather than metabolic substrate loss, it may be beneficial to both restrict mitochondrial respiration and boost glycolysis[43,44]. A compound such as *Uca*C3F8F3 may have more potential in this context. This is supported by the reduction in the size of lesion in explants treated with *UcAC3F8f3* prior to insult in a pig explant model of AMD.

Among the estimated 150-190 species within the genus Uvaria of Annonaceae, several are sources of acetogenins with inhibitory effects on mitochondrial complex I[45]. The acetogenins from this plant family are considered broadly neurotoxic and they would not emerge as an obvious candidate for ocular treatment unless an unbiased screen were to uncover them. Moreover, the amphiphilic properties of acetogenins make them moderately permeable, which means smaller acetogenin-like compounds (<400 Da) could show potential to cross the corneal, stromal and vitreous barriers to reach the retina upon topical application. Topical drug-delivery to the retina is particularly challenging as any compound would need to be sufficiently lipophilic to cross the corneal epithelium while also having enough hydrophilicity to cross the stroma and remain inert enough not to interact with tear proteins along the way. The few molecules that have shown this goldilocks capacity, such as resveratrol and curcumin metabolites, are plant-derived but have insufficient bio-availability after crossing the aqueous and vitreous humors. This makes the wide-net screen such as we have carried out in this study of interest for finding topical treatments for RD. However, a limitation of the study is our heavy reliance on the index of survival in a pure cone culture, rather than in a multi-cellular retinal-based platform. An example of the latter is the glucose-deprived retinal organoid used in a recent screen for chemogenetic cone-protective probes[46]. This study demonstrated how retinal organoids have become more scalable and therefore adaptable to HCS over the last five years. Screening a smaller library of selected phytochemical compounds on retinal organoids may offer other promising candidates for cone protection. Extracts of the Annonaceae plant family may be particularly suited for such selective screening, as compounds derived from these plants are prevalent in the pharmaceutical industry and have multiple pharmacological functions[47]. Today synthetic compounds can be designed for a specific molecular target using combinatorial chemistry filtered through a computational-heavy pipeline, making it seem unnecessary to screen plant extracts. Plant-derived natural compounds cannot be patented so there is little commercial compensation for the arduous pipeline of field collection, extraction, fractionation, followed by potency and toxicity assays [10]. However, nature

has had millenia to evolve molecules that modulate metabolic activities of living cells, and it is estimated that only a fraction of natural compounds that could become first-in-class therapeutics have been found[46]. Natural structures remain one of the richest sources of chemical novelty, which means its sometimes of value to go back to find cures in plants or at least to find original chemical templates, such as the open-lactone ring acetogenin we describe here.

METHODS

Cone culture platform

Fertilized eggs from chickens (Morizeau farm, Eure-et-Loir) were collected post-laying and stored at 17°C until use. For each experiment, 7 eggs were incubated (24 h at 20°C, then 136 h at 37°C with intermittent tilting) to reach stage 29 (6.5 days). Eggs were surface-disinfected (Pursept A express), shells opened, and embryos transferred into 37°C PBS; amnions were removed to confirm staging. Two stage-29 embryos were decapitated and enucleated, and the four eyes placed in CO2-independent medium. Retinas were isolated by inserting fine forceps at the optic nerve, separating the retina from the RPE, then removing cornea, lens, and vitreous. Retinas were transferred to Ringer's solution, finely dissected, washed twice, and digested with 0.25% trypsin (20 min, 37°C). Digestion was stopped with M199 + 10% FBS, and released DNA was digested with DNase I (0.012 mg/retina). Cell clumps were dissociated by repeated pipetting, then washed twice in chemically defined medium (CDM; M199/DMEM 1:1, supplemented with insulin, transferrin, Na2SeO3, putrescine, progesterone, prostaglandin, taurine, CDP-choline, CDP-ethanolamine, hydrocortisone, T3, sodium pyruvate, and gentamicin). Cells were resuspended in CDM, and viable cell concentration was determined using a Malassez hemocytometer with trypan blue exclusion. Poly-L-lysine-coated (32.25 µg/cm²) 96-well black clear-bottom plates (Corning 3603) were seeded with 50 µl of cell suspension at 1×10^5 or 2×10^5 cells/cm², using a multichannel pipette and a predefined plate layout to ensure homogeneous distribution and minimize reading artifacts.

Plant High Content Screen

Two hundred plants were selected for the HCS based on their tropical biodiversity and their presence in traditional tropical pharmacopoeia databases including the Duke database and the Royal Botanical gardens database (Table S1) [27]. Four types of extract from either leaf, bark grain or fruit were made in either polyamide methanol, ethyl acetate, depleted ethyl acetate and depleted methanol. This yielded 800 extracts with each extract tested at two concentrations, 10 and 100 µg/ml, and each concentration tested on two chicken cone cell densities, ($1x10^5$ and $2x10^5$ cells/cm^2) giving 3,200 distinct tests. In addition, four independent measures were made for each extract at each concentration yielding a total of 12,800 tests that were plated. The plant extracts were generated by our industry collaborators, GreenPharma and plated onto the 96-well chicken cone cultures in a format to ensure an unbiased screen (Fig. 1D). The selection criterion was the viability factor: the average cone survival across 4 replicate wells divided by the average

survival across 19 negative control wells. A viability factor ≧2 was chosen arbitrarily as the cut-off. Ultimately, two hundred 96-well plates requiring 700 fertilized chicken eggs were used to produce the full data which is presented in https://data.mendeley.com/datasets/2752kfkxf2/1.

Preparing Plant extracts

Plant materials were extracted using an ASE 200 system (Dionex) under nitrogen (6–8 bar). Four extract types were prepared: methanolic polyamide (MP), ethyl acetate (EA), depleted ethyl acetate (DEA), and depleted methanol (DM). For MP extraction, 5–6 g of powdered plant material was mixed with 5 g of polyamide (SC6, Macherey-Nagel), 10 g of plant material was used for EA, DEA, and DM extractions. DEA and DM preparations included a preliminary heptane depletion step, followed by extraction with ethyl acetate or methanol, respectively.
Extractions were performed at 60°C using four 3-min cycles for MP and five 3-min cycles for EA, DEA, and DM, followed by a 60% solvent flush and a 120-s nitrogen purge. Extracts were collected, concentrated at 40°C under reduced pressure using a Büchi rotary evaporator, reconstituted in water, and lyophilized for 48 h. A library comprising 800 extracts from 200 plant species was generated. An aliquot of 2 mg of each dried extract was transferred into individual 4-mL glass vials, uniquely coded, and stored at −80°C. Extraction yield was determined gravimetrically as the ratio of dried extract mass to initial plant material mass × 100.

Small-Scale Fractionation of UcMP by Reversed-Phase SPE

For small-scale fractionation, UcaC was suspended in water (10 mg mL^{-1}) by vortex mixing and sonication for 5 min. Sonication was repeated twice, with incubation at 42°C for 30 min The resulting suspension was sequentially filtered through Whatman Grade 4 (20–25 µm) and Grade 3 (6 µm) filter papers, followed by glass-fiber filtration (GFB/F, 0.7 µm; alternatively GFB/B, 1.0 µm) and a final 0.22-µm polyethersulfone membrane. Reversed-phase solid-phase extraction (SPE) was performed using C18-E Strata cartridges (55 µm, 70 Å; 10-g sorbent capacity). Cartridges were conditioned sequentially with methanol (100 ml) and water (60 ml). Approximately 50 mL of the aqueous UcMP preparation, corresponding to 500 mg of extract, was loaded onto the cartridges under controlled vacuum (20–40 mbar) at a flow rate of approximately 1 mL min^{-1}. Three fractions were obtained by sequential elution: UcAC1 with 50 mL demineralized water, UcAC2 with 60 ml methanol/water (40:60, v/v), and UcAC3 with 60 mL methanol. The cartridges were dried under vacuum between successive elution steps. UcAC1 was frozen at −80°C and lyophilized to dryness. UcMAC2 and UcAC3 were concentrated at 40°C under reduced pressure (70–50 mbar) using a Büchi rotary evaporator, frozen at −80°C, and subsequently lyophilized to dryness.
UcMPC3 was subsequently fractionated by reversed-phase HPLC into eight fractions using an optimized methanol/water gradient. Separation was performed on a C18 column (250 × 4.6 mm, 5 µm, 100 Å) maintained at 30°C. The gradient was maintained at 80% methanol for 3 min, followed by a linear increase to 100% methanol over 13 min and a subsequent hold at 100% methanol for 22 min. For semi-preparative separation, 250 µl of UcMPC3 (2.5 mg) was injected at a flow rate of 4 mL min^{-1}, and the eight fractions were collected using an automated Foxy Jr collector.

Phytocompound purification: Mass spectrometry

Ionization was achieved by electrospray ionization (ESI) for the mass spectrometer to separate them by mass-to-charge ratio (m/z). Analyses were performed on a Finnigan MAT LCQ HPLC-MS system comprising a degasser, a P4000 quaternary pump (four solvent channels, 1 ml/min), an AS3000 autosampler, and a UV6000LP photodiode-array detector, with absorbance monitored at 220, 254, 330, and 400 nm (190–800 nm range) using deuterium and tungsten lamps. Separation was performed on a Kromasil 100-5C18 column (5 µm, 250 × 4.6 mm), maintained at 30°C. Ions were generated in the source under a constant flow of 99% pure nitrogen (6.9 bar), operating in both positive (ESI+) and negative (ESI–) modes, with the capillary held at 200°C; the mobile phase was acidified with 0.01% formic acid to facilitate ionization. Mass analysis was performed using a quadrupole analyzer scanning from 50.00 to 2000.00 Da, controlled by LCQ-Tune software. Mass values were cross-referenced with chromatographic profiles, and ion abundance was represented as either continuous spectra (peak traces) or fragmentation spectra (histograms of relative ion intensity vs. m/z). From these spectra, information was obtained on the mass, UV absorption spectrum, retention time, ESI+/ESI– detection mode, and presence of sodium or formic adducts or divalent/trivalent ion forms for abundant ions.

Glucose uptake assay

Cone-enriched cultures prepared from the retinas of chicken embryos at stage 29 were incubated in the presence of the UcAC3F8f3S4 fractions at 100 ng/ml. After 4 days of in vitro incubation, the culture medium was replaced with 100 µl of glucose-free medium containing phenol red in a medium containing 2 mM glutamine and the supplements. After 1 hour of incubation, the cells were washed, and the fluorescent glucose analog, 2-N-7-Nitrob enz-2-oxa-1,3-diazol-4-ylAmino-2-Deoxyglucose (2-NBDG, Life technologies) was added at a final concentration of 150 µM. After 10 minutes of incubation at 37°C, the culture medium was removed and the cells were washed. The fluorescence of the cells was measured after excitation at 485 nm by detecting the emission at 520 nm.

Retinal and RPE explants

Pig eyes were dissected within 2 hours of reception from the abattoir. The retinas were dislodged from the eye-cup using cooled dPBS before transfer to CO_2-independent media (Gibco) for further dissection. Retinal explants were cultured for up to 1 week with the phytocompounds.

Eye-cups containing sclera, choroid and RPE were dissected in the same media before the extraction of 2mm^2 biopsies using disposable biopsy punches (Integra, Miltex) and transferred to 24-well plates with complete DMEM (Gibco) and 10% serum for immediate imaging.

Alternatively, RPE cells were dissociated from the eye-cups by incubation with 0.25% trypsin for 30 minutes at 37°C. The cells were resuspended after centrifugation (250xg for 5 minutes) in 9.75ml of cell culture medium containing 20% serum. The cell solution was divided across 65 wells of a 96-well plate for the TMRM study.

For the PNA-labelled lesion analysis, images were taken using the 594nm laser on a Yokogawa CQ1, spinning disk microscope (20× objective) and each field analyzed in Python (see Analysis software).

Mitochondrial membrane potential assay

The TMRM-induced responses of RPE cells in explanted pig eye-cups were initially measured at the single-cell level by time-lapse imaging on a CQ1 double spinning-disk microscope with(Yokogawa CSU-W1) with the effects of the Complex V blocker oligomycin and the uncoupler FCCP used to reveal mitochondrial complex activity in the RPE (Supplementary Fig. S3). For phytocompound tests, the RPE cells were isolated from pig eye-cups and seeded at 4.0E4 per well of a 96-well for 6 hours until they were adhered to the bottom of the plate. Cells were then treated with the phytocompounds and incubated overnight. For membrane potential measurement cells were exposed to a mix of 50nM TMRM (Thermofisher scientific, T668) and Mitotracker Deep Red (Thermofisher scientific, M22426) for 40 minutes at 37°C. A Spark plate-reader (Tecan) was used for kinetic measurements at 542 nm every minute over 5 minutes upon each drug addition, with a final reading at 647 nm to record mitotracker levels. The readings were normalised to the level mitotracker fluorescence in each well.

Analysis software and statistical methods

Cone counts were carried out using the CellVoyager HCS analysis system (Yokogawa).

Graphpad (Prism) was used to support statistical analyses on figure 1, 2, 4, and 5. Python scripts in Jupyterlab (Anaconda) was used to analyse TMRM data. To analyse lesion data, scripts were written in python with assistance of Cursor (Claude 3.5 Sonnet / GPT-4o). This involved a first step of Top-hat filtering (σ = 2 px) to emphasize cone-sized bright puncta with peak detection, followed by a dark lesion and void mask where macro-normalized fluorescence was below the 2nd percentile of tissue values. All logic, outputs, and numerical results have been fully verified by the authors.

FIGURE LEGENDS

Figure 1 Identification of an extract from Uvaria chamae protecting cones by high content screening on cone-enriched cultures from chicken embryo.

(A) The developmental stage 29 of chicken embryos from which the retinal cone cultures are established is boxed in red in the developmental embryology schema. (B) The rate of cone photoreceptor death is measured over the week at two different cell seeding densities (LHS). On corresponding days cell bodies and axons were stained with the chicken specific cone marker visinin (RHS). (C) One plant extract (*Fructus barbarum*), its two major cytoprotective constituents (Lutein and Zeaxantin), their equimolar mix (Zeaxantin + Lutein) and an additional retina-protective published plant molecule (Resveratrol) were tested for cone protection to establish a benchmarking control[5]. (D) Schema showing the experimental work-flow involving generation of plant extracts, cone-enriched cultures, high-throughput screen and final analysis using a viability factor cut-off. (E) Each of the 30 top-performing plant extracts selected from a first screen were compared in a cytoprotective (green bars) versus cytotoxic (red bars) screen on two cell densities. The different compound formulations are listed across the rows depending on whether they were extracted in either methanol (MP), Ethyl acetate (EA), Depleted Ethyl Acetate (DEA) or Depleted Methanol (DM).

Figure 2 *UcAC3F8f3* is purified from the Uvaria chamae extract

(A) The cone protective effects of leaf extracts from the four species of Uvaria Chamae (*Uc*a, *Uc*b, *Uc*c and *Uc*d) tested at concentrations of 1 and 100 µg/ml. (B) Sequential reverse-phase chromatography steps at increasing methanol (MEOH) concentrations was used to fractionate Uca into *Uca*C1 (blue trace) under aqueous conditions (0% MEOH), *Uca*C2 (green trace) pulling out moderately non-polar compounds (40% MEOH), *Uca*C3 (red trace) pulling out non-polar/lipophilic compounds (100% MEOH) as well as a the whole extract (grey trace). (C) Cone-protective effect of *Uc*aC1, *Uc*aC2 and *Uc*aC3 fractions with the combined fraction, *Uca* at concentrations 100 µg/ml, and the vehicle control, 0. (D) Chromatogram of the fractionation by reverse phase HPLC under increasing methanol of the fraction *Uc*aC3. The eight fractions (*Uc*ac3F 1-8) are indicated by grey/white shading. (E) The 8 subfractions compared for cone-protective effects against the whole *Uc*aC3 fraction and 0, as a vehicle control. (F) The chromatogram profile of three further subfractions of UcaC3f8 with f1 (green trace) at 60% MEOH, f2 (green trace) at 80% MEOH and f3 (red trace) at 100% MEOH and the black trace as the unfractionated extract (G) The 3 subfractions f1, f2, f3 compared for cone protective effects at 0.1 and 10µg/ml with 0, as a vehicle control and F8 as the unfractionated extract. (H) A summary of the consecutive fractionation steps to produce an upscaled cytoprotective product of increasing purity from the initial protective *Uc* fraction. The final step 5 products were used for structure-activity analysis by mass-spec (I) Analysis of the effect of cone cell morphology in cone-enriched cultures after 1 week of incubation with 50ng/ml of *UcAC3F8f3*. Cells are labeled with calcein AM. Neurite extensions are distinguished with yellow arrows. *MEOH: Methanol, ****p<0.0005*

Figure 3 *UcAC3F8f3* has a modest dose-dependent direct effect on mitochondrial function. (A) Chromatographic profile of the original Uc plant extract (B) Final fraction with a selected image from the ^{1}H-^{1}H COSY NMR spectrum on top. The diagonal line represents the uncoupled proton signals, highlighting the characteristic structural features of the acetogenin core, including the tetrahydrofuran (THF) ring zone (3.4-4.0 ppm), the terminal γ-lactone moiety (~ 5.0 and ~ 7.0 ppm), and the major aliphatic lipid chain (0.8-1.5 ppm). The final elucidated structure ($C_{37}H_{66}O_7$) is shown below with epoxy (*epo*), ring connectivity (*R* and *R'*), furane (*F*) and gamma lactone substructures listed. (C) RPE cells dissociated from pig eyes are shown after 24 hours of culturing with *UcAC3F8f3* (lower panel) or with vehicle-only Control (top panel). (D) Snapshot of pig RPE cells in explant biopsies during live cell imaging with TMRM (purple cells, middle panel) and Mitotracker (green cells, top panel) (E) Mitochondrial membrane potential (ΔΨm) of the negative vehicle-only control 'No Treatment' and a positive control for complex I inhibition '250nM Rotenone' were compared to concentrations from 1000 to 0.01 µg/ml of *UcAC3F8f3* using TMRM (50nM) and mitotracker. Fluorescence measures taken before, '-' and after, '+' treatment with membrane uncoupler FCCP (1.5 µM). Eyes from four animals were used in each of two experiments and the results pooled. The 8 distinct conditions were tested across wells containing cells from the same eye. The Rotenone condition was only included in the second experiment. (F) Schematic representation of the site of interaction of 2-Cyano-3-(1-phenyl-1H-indol-3-yl)-2-propenoic acid (UK5099). (G) The *Uc*AC3F8f3-mediated chicken cone protection was assessed

compared to the positive control, Fb, showing protective effect persists in the absence or presence of increasing dose of UK5099 from 5 to 50 ng/ml. *ns: Not Significant, ***p<0.0005, ****p<0.0005*

Figure 4 *Uc*AC3F8f3 protective effect on cones is inhibited by blocking aerobic glycolysis. (A) Cell protection by *Uc*AC3F8f3 at 100 µg/ml on cone-enriched cultures incubated in 15 versus 30 mM glucose. (B) Uptake of plasmid-derived NBDG, a fluorescent derivative of deoxyglucose (structure shown in boxed inset), by *Uc*AC3F8f3 compared to a plasmid control (pcDNA3-0). (C) Schema for inhibition of the conversion of pyruvate, PYR to lactate, LACT, by oxamate, a lactate dehydrogenase inhibitor. (D) Protection of cones in cone-enriched cultures in the presence '+' or absence '–' of *Uc*AC3F8f3 at 100 µg/ml and with increasing concentrations of oxamate from 0 to 25 nM. ***p<0.005, ***p<0.0005, ****p<0.00005*

Figure 5 *Uc*AC3F8f3 protects cones by stimulating aerobic glycolysis at the phosphofructokinase catalytic node.
(A) Schema for the glycolytic pathway intersecting with oxidative phosphorylation and aerobic glycolysis with arrows pointing to mass-spectrometry supported analysis of key metabolites following treatment of chick cone-enriched cultures with (+) and without (-) *Uc*AC3F8f3. (B) The expression levels of the enzyme *PFKFB2* in chick cone-enriched culture incubated with 15 versus 30mM glucose. (C) Expression of *PFKFB2* in chick cone-enriched culture incubated with (+) and without (-) 10ng/ml of *Uc*AC3F8f3. (D) *Uc*AC3F8f3-mediated protection of cones is enhanced after electroporation of a plasmid encoding mouse *Pfkfb2*.
PFKFB2: 6-phosphofructo-2-kinase/fructose-2,6-biphosphatase 2; **p<0.05, **p<0.005, ***p<0.0005, ****p<0.00005*

Figure 6 Atrophic lesions in a pig model of geographic atrophy are reduced by *Uc*AC3F8f3 treatment
(A) Retinas explanted from *rd*1 mice at PN day 21 (schema on LHS) are cultured for 1 week with 1.5µg total of *Uc*AC3F8f3 extract and show no increase in PNA-labelled cone counts compared to vehicle controls (B) Schema of the pig retinal flat-mount (top). Image of PNA-lectin stained cone outer segments from pig retinal explant (lower LHS panel) with the corresponding image from the lesion-delineating software (lower RHS panel). (C) Box-plots showing the number of atrophic hypofluorescent (≥80 µm in diameter) and hole-like lesions on the explants and (D) lesion size (%age of the surface area) (E) Flat-mounted biopsies from pig retinal explants untreated 'Healthy control', or treated with an inhibitor 'transport inhibitor' and tested against vehicle 'Vehicle control' or *Uc*AC3F8f3 at concentrations of 10ng, 10µg or 100µg. *FOV: Field of View; PN: Post-Natal; RD: Retinal degeneration; p<0.05**

Figure S1 HCS Plate format
96-well Plate layout for the HCS screen of 800 different plant extracts for chicken cone cell survival. The positive control, Fb, is shown at the top row A1-A4 with remaining wells containing leaf extracts from the plant extract library, at concentrations of 100 and 10 (µg/ml), or containing vehicle controls, 0. Each concentration was tested on two chicken cone cell

densities, ($1x10^5$ and $2x10^5$ cells/cm^2) with four independent measures were made for each extract at each concentration.

Figure S2 Phylogenetic analysis of the high content screening results.
In black are all plants that have been screened. In grey are plants phylogenetically close to a screened plant. In red are two Annonaceae that have been shown to protect cones from cone-enriched cultures (*Annona Senegalensis* (*) and *Uvaria Chamae* (**)) following high content screening.

Figure S3 Cone protection by Uca fractions following liquid-liquid HPLC
The cytoprotective activity polar, apolar and alkaloid chemical subfractions of the UcAC3F8 fraction were tested on cone-enriched cultures of $10^5/cm^2$. The apolar and alkaloid fractions were also tested in a 1:1 mix.

Figure S4 Mitochondrial membrane potential recording from pig retinal explants

TMRM quenching profile recorded by time-lapse imaging of $2mm^2$ biopsies of pig explants containing RPE, choroid and sclera. The images were recorded every 30 seconds over an hour on a CQ1 spinning disk microscope and Benchtop analysis system (CQ1 Yokogawa).

Declaration of interests

The compound described here is the subject of a patent issued to the authors in 2023: WO2023139091A1

Declaration of AI-assisted technologies in the manuscript preparation process

During the preparation of this work, the authors used Cursor (Claude 3.5 Sonnet / GPT-4o) for image analysis. The authors reviewed and edited the output as needed and take full responsibility for the content of the published article.

Author contributions

AB, GP, MC and EG purified compounds by HPLC, carried out the phytocompound screens and metabolic analyses; FB performed bioinformatic analyses; TC and VF performed the pig explant work and mitochondrial analyses and imaging; IA, CZ, TL, PB and FH supervised staff and students working on the project; JS, SP TL and FH conceived of this project and obtained funding for the work. TC wrote the manuscript and all authors edited the manuscript.

Acknowledgements

The authors thank the MetaToul platform (Toulomics / Metabolomics and Fluxomics Core Facility, Toulouse, France), an IBiSA-certified facility and member of the national infrastructure MetaboHUB, for technical expertise and access to analytical equipment/tools in particular Jean Charles Portet, Floriant Bellvert, Lara Gales. We also wish to thank the Animal Facility of the Institut de la Vision (Paris, France) for their technical assistance, support, and care of the animal models used in this study, in particular Manuel Simonutti and Julie Degardin.

REFERENCES

1. Pelner, L. Garcia da Orta. *JAMA* **197**, 996–998 (1966).
2. Basma, J. *et al.* Legacy of Syriac-Aramaic Scholars in Transmitting Neurosurgical Knowledge Between Antiquity and the Middle Ages. *World Neurosurg* **152**, 71–79 (2021).
3. Leffler, C. T. *et al.* Enduring Influence of Elizabethan Ophthalmic Texts of the 1580s: Bailey, Grassus, and Guillemeau. *Open Ophthalmol J* **8**, 12–18 (2014).
4. Packer, M. & Brandt, J. D. Ophthalmology's botanical heritage. *Surv Ophthalmol* **36**, 357–365 (1992).
5. Age-Related Eye Disease Study 2 Research Group. Lutein + zeaxanthin and omega-3 fatty acids for age-related macular degeneration: the Age-Related Eye Disease Study 2 (AREDS2) randomized clinical trial. *JAMA* **309**, 2005–2015 (2013).
6. Keenan, T. D. L. *et al.* Oral Antioxidant and Lutein/Zeaxanthin Supplements Slow Geographic Atrophy Progression to the Fovea in Age-Related Macular Degeneration. *Ophthalmology* **132**, 14–29 (2025).

7. Bosch-Morell, F. *et al.* Medicinal plants and natural products as neuroprotective agents in age-related macular degeneration. *Neural Regen Res* **15**, 2207–2216 (2020).
8. Aït-Ali, N. *et al.* Rod-derived cone viability factor promotes cone survival by stimulating aerobic glycolysis. *Cell* **161**, 817–832 (2015).
9. Chen, Y. *et al.* Retinal metabolism displays evidence for uncoupling of glycolysis and oxidative phosphorylation via Cori-, Cahill-, and mini-Krebs-cycle. *Elife* **12**, RP91141 (2024).
10. Du, J. *et al.* Phototransduction Influences Metabolic Flux and Nucleotide Metabolism in Mouse Retina. *J Biol Chem* **291**, 4698–4710 (2016).
11. Kanow, M. A. *et al.* Biochemical adaptations of the retina and retinal pigment epithelium support a metabolic ecosystem in the vertebrate eye. *Elife* **6**, e28899 (2017).
12. Hurley, J. B., Lindsay, K. J. & Du, J. Glucose, lactate, and shuttling of metabolites in vertebrate retinas. *J Neurosci Res* **93**, 1079–1092 (2015).
13. Léveillard, T. *et al.* Identification and characterization of rod-derived cone viability factor. *Nat Genet* **36**, 755–759 (2004).
14. Chan, H.-C. *et al.* Neuroprotective effects of Lycium barbarum Lynn on protecting retinal ganglion cells in an ocular hypertension model of glaucoma. *Exp Neurol* **203**, 269–273 (2007).
15. Popoola, T. D. *et al.* Potent Nrf2-inducing, antioxidant, and anti-inflammatory effects and identification of constituents validate the anti-cancer use of Uvaria chamae and Olax subscorpioidea. *BMC Complement Med Ther* **21**, 234 (2021).
16. Okokon, J. E., Ita, B. N. & Udokpoh, A. E. The in-vivo antimalarial activities of Uvaria chamae and Hippocratea africana. *Ann Trop Med Parasitol* **100**, 585–590 (2006).

17. Adler, R. & Hatlee, M. Plasticity and differentiation of embryonic retinal cells after terminal mitosis. *Science* **243**, 391–393 (1989).
18. Millet-Puel, G. *et al.* Cone-Enriched Cultures from the Retina of Chicken Embryos to Study Rod to Cone Cellular Interactions. *J Vis Exp* https://doi.org/10.3791/61998 (2021) doi:10.3791/61998.
19. Fintz, A.-C. *et al.* Partial characterization of retina-derived cone neuroprotection in two culture models of photoreceptor degeneration. *Invest Ophthalmol Vis Sci* **44**, 818–825 (2003).
20. Zhang, Q., Chen, W., Zhao, J. & Xi, W. Functional constituents and antioxidant activities of eight Chinese native goji genotypes. *Food Chem* **200**, 230–236 (2016).
21. Amagase, H. & Nance, D. M. Lycium barbarum increases caloric expenditure and decreases waist circumference in healthy overweight men and women: pilot study. *J Am Coll Nutr* **30**, 304–309 (2011).
22. Handelman, G. J., Dratz, E. A., Reay, C. C. & van Kuijk, J. G. Carotenoids in the human macula and whole retina. *Invest Ophthalmol Vis Sci* **29**, 850–855 (1988).
23. Snodderly, D. M. Evidence for protection against age-related macular degeneration by carotenoids and antioxidant vitamins. *Am J Clin Nutr* **62**, 1448S-1461S (1995).
24. Kiani, A. K. *et al.* Flavonoid supplements increase neurotrophin activity to modulate inflammation in retinal genetic diseases. *Acta Biomed* **91**, e2020014 (2020).
25. Liu, S.-Y. *et al.* Resveratrol protects photoreceptors by blocking caspase- and PARP-dependent cell death pathways. *Free Radic Biol Med* **129**, 569–581 (2018).

26. Wiedemann, J., Rashid, K. & Langmann, T. Resveratrol induces dynamic changes to the microglia transcriptome, inhibiting inflammatory pathways and protecting against microglia-mediated photoreceptor apoptosis. *Biochem Biophys Res Commun* **501**, 239–245 (2018).
27. Slik, J. W. F. *et al.* An estimate of the number of tropical tree species. *Proc Natl Acad Sci U S A* **112**, 7472–7477 (2015).
28. Lannuzel, A. *et al.* The mitochondrial complex I inhibitor annonacin is toxic to mesencephalic dopaminergic neurons by impairment of energy metabolism. *Neuroscience* **121**, 287–296 (2003).
29. Escobar-Khondiker, M. *et al.* Annonacin, a natural mitochondrial complex I inhibitor, causes tau pathology in cultured neurons. *J Neurosci* **27**, 7827–7837 (2007).
30. Kaboré, K. *et al.* Phenolic Content, Antioxidant Potential, and Antimicrobial Activity of Uvaria chamae (Annonaceae), a Food Plant from Burkina Faso. *Biochem Res Int* **2024**, 1289859 (2024).
31. Aparicio, A., Camacho, E. T., Philp, N. J. & Wirkus, S. A. A mathematical model of GLUT1 modulation in rods and RPE and its differential impact in cell metabolism. *Sci Rep* **12**, 10645 (2022).
32. Chandler, L. C., Gardner, A. & Cepko, C. L. RPE-specific MCT2 expression promotes cone survival in models of retinitis pigmentosa. *Proc Natl Acad Sci U S A* **122**, e2421978122 (2025).
33. Hass, D. T. *et al.* In vivo exchange of glucose and lactate between photoreceptors and the retinal pigment epithelium. Preprint at https://doi.org/10.1101/2023.04.10.536306 (2024).

34. Coffe, V., Carbajal, R. C. & Salceda, R. Glucose metabolism in rat retinal pigment epithelium. *Neurochem Res* **31**, 103–108 (2006).
35. Nisselbaum, J. S., Packer, D. E. & Bodansky, O. Comparison of the actions of human brain, liver, and heart lactic dehydrogenase variants on nucleotide analogues and on substrate analogues in the absence and in the presence of oxalate and oxamate. *J Biol Chem* **239**, 2830–2834 (1964).
36. Chinchore, Y., Begaj, T., Wu, D., Drokhlyansky, E. & Cepko, C. L. Glycolytic reliance promotes anabolism in photoreceptors. *Elife* **6**, e25946 (2017).
37. Minchenko, O., Opentanova, I. & Caro, J. Hypoxic regulation of the 6-phosphofructo-2-kinase/fructose-2,6-bisphosphatase gene family (PFKFB-1-4) expression in vivo. *FEBS Lett* **554**, 264–270 (2003).
38. Bockus, L. B. *et al.* Cardiac Insulin Signaling Regulates Glycolysis Through Phosphofructokinase 2 Content and Activity. *J Am Heart Assoc* **6**, e007159 (2017).
39. Pittler, S. J. & Baehr, W. Identification of a nonsense mutation in the rod photoreceptor cGMP phosphodiesterase beta-subunit gene of the rd mouse. *Proc Natl Acad Sci U S A* **88**, 8322–8326 (1991).
40. Clérin, E. *et al.* e-conome: an automated tissue counting platform of cone photoreceptors for rodent models of retinitis pigmentosa. *BMC Ophthalmol* **11**, 38 (2011).
41. Sans, C. L., Satterwhite, D. J., Stoltzman, C. A., Breen, K. T. & Ayer, D. E. MondoA-Mlx heterodimers are candidate sensors of cellular energy status: mitochondrial localization and direct regulation of glycolysis. *Mol Cell Biol* **26**, 4863–4871 (2006).

42. Peterson, C. W., Stoltzman, C. A., Sighinolfi, M. P., Han, K.-S. & Ayer, D. E. Glucose controls nuclear accumulation, promoter binding, and transcriptional activity of the MondoA-Mlx heterodimer. *Mol Cell Biol* **30**, 2887–2895 (2010).
43. Sekiguchi, K., Murai, M. & Miyoshi, H. Exploring the binding site of acetogenin in the ND1 subunit of bovine mitochondrial complex I. *Biochim Biophys Acta* **1787**, 1106–1111 (2009).
44. Clérin, E. *et al.* Combined Expression of hRdCVF and hRdCVFL Through AAV-Mediated Delivery for the Treatment of Retinitis Pigmentosa. *Invest Ophthalmol Vis Sci* **67**, 2 (2026).
45. Dahiya, R. & Dahiya, S. Natural bioeffective cyclooligopeptides from plant seeds of Annona genus. *Eur J Med Chem* **214**, 113221 (2021).
46. Muthuraj, R. & Chandrasekaran, J. Nature meets machine: the AI renaissance in natural product drug discovery. *Nat Prod Bioprospect* **16**, 37 (2026).

FIGURE 1

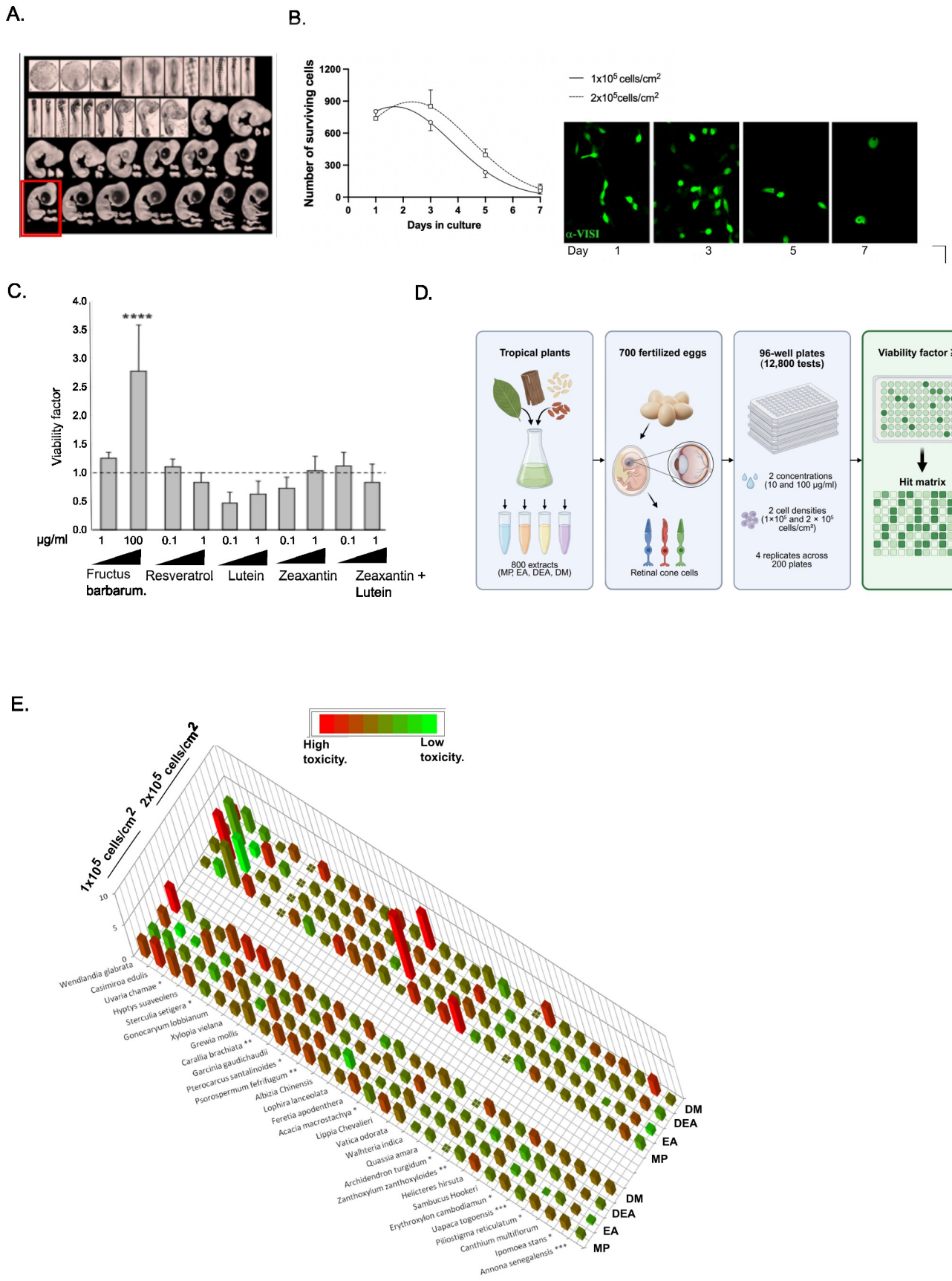

A.
B.
Number of surviving cells
1200
900
600
300
0
0 1 2 3 4 5 6 7
Days in culture
1x10⁵ cells/cm²
2x10⁵cells/cm²
α-VISI
Day 1 3 5 7
C.
Viability factor
4.0
3.5
3.0
2.5
2.0
1.5
1.0
0.5
0.0
****
µg/ml
1 100 0.1 1 0.1 1 0.1 1 0.1 1
Fructus barbarum.
Resveratrol
Lutein
Zeaxantin
Zeaxantin + Lutein
D.
Tropical plants
800 extracts (MP, EA, DEA, DM)
700 fertilized eggs
Retinal cone cells
96-well plates (12,800 tests)
2 concentrations (10 and 100 µg/ml)
2 cell densities (1×10⁵ and 2 × 10⁵ cells/cm²)
4 replicates across 200 plates
Viability factor ≥ 2
Hit matrix
E.
High toxicity.
Low toxicity.
1x10⁵ cells/cm²
2x10⁵ cells/cm²
10
5
0
Wendlandia glabrata
Casimiroa edulis
Uvaria chamae *
Hyptys suaveolens
Sterculia setigera *
Gonocaryum lobbianum
Xylopia vielana
Grewia mollis
Carallia brachiata **
Garcinia gaudichaudii
Pterocarcus santalinoides *
Psorospermum febrifugum **
Albizia Chinensis
Lophira lanceolata
Feretia apodenthera
Acacia macrostachya *
Lippia Chevalieri
Vatica odorata
Walhteria indica
Quassia amara
Archidendron turgidum *
Zanthoxylum zanthoxyloides **
Helicteres hirsuta
Sambucus Hookeri
Erythroxylon cambodianum *
Uapaca togoensis ***
Piliostigma reticulatum *
Canthium multiflorum
Ipomoea stans *
Annona senegalensis ***
DM
DEA
EA
MP
DM
DEA
EA
MP

Figure 2

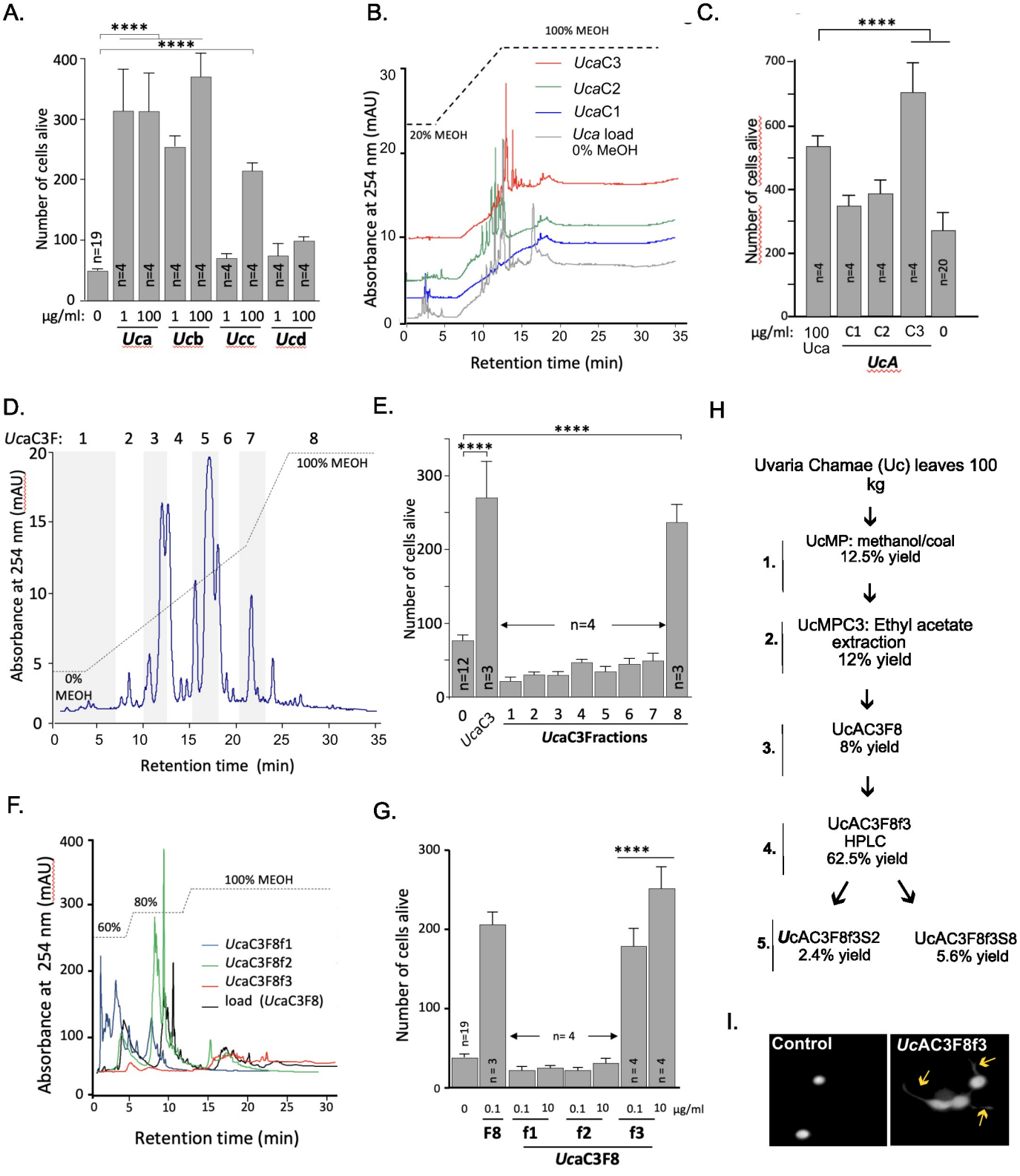

A.
Number of cells alive
µg/ml: 0 1 100 1 100 1 100 1 100
Uca Ucb Ucc Ucd
B.
100% MEOH
UcaC3
UcaC2
UcaC1
Uca load
0% MeOH
20% MEOH
Absorbance at 254 nm (mAU)
Retention time (min)
C.
Number of cells alive
µg/ml: 100 C1 C2 C3 0
Uca
UcA
D.
UcaC3F: 1 2 3 4 5 6 7 8
100% MEOH
0% MEOH
Absorbance at 254 nm (mAU)
Retention time (min)
E.
Number of cells alive
n=4
UcaC3
UcaC3Fractions
H
Uvaria Chamae (Uc) leaves 100 kg
1. UcMP: methanol/coal 12.5% yield
2. UcMPC3: Ethyl acetate extraction 12% yield
3. UcAC3F8 8% yield
4. UcAC3F8f3 HPLC 62.5% yield
5. UcAC3F8f3S2 2.4% yield
UcAC3F8f3S8 5.6% yield
F.
100% MEOH
80%
60%
UcaC3F8f1
UcaC3F8f2
UcaC3F8f3
load (UcaC3F8)
Absorbance at 254 nm (mAU)
Retention time (min)
G.
Number of cells alive
n= 4
µg/ml
F8 f1 f2 f3
UcaC3F8
I.
Control
UcAC3F8f3

Figure 3

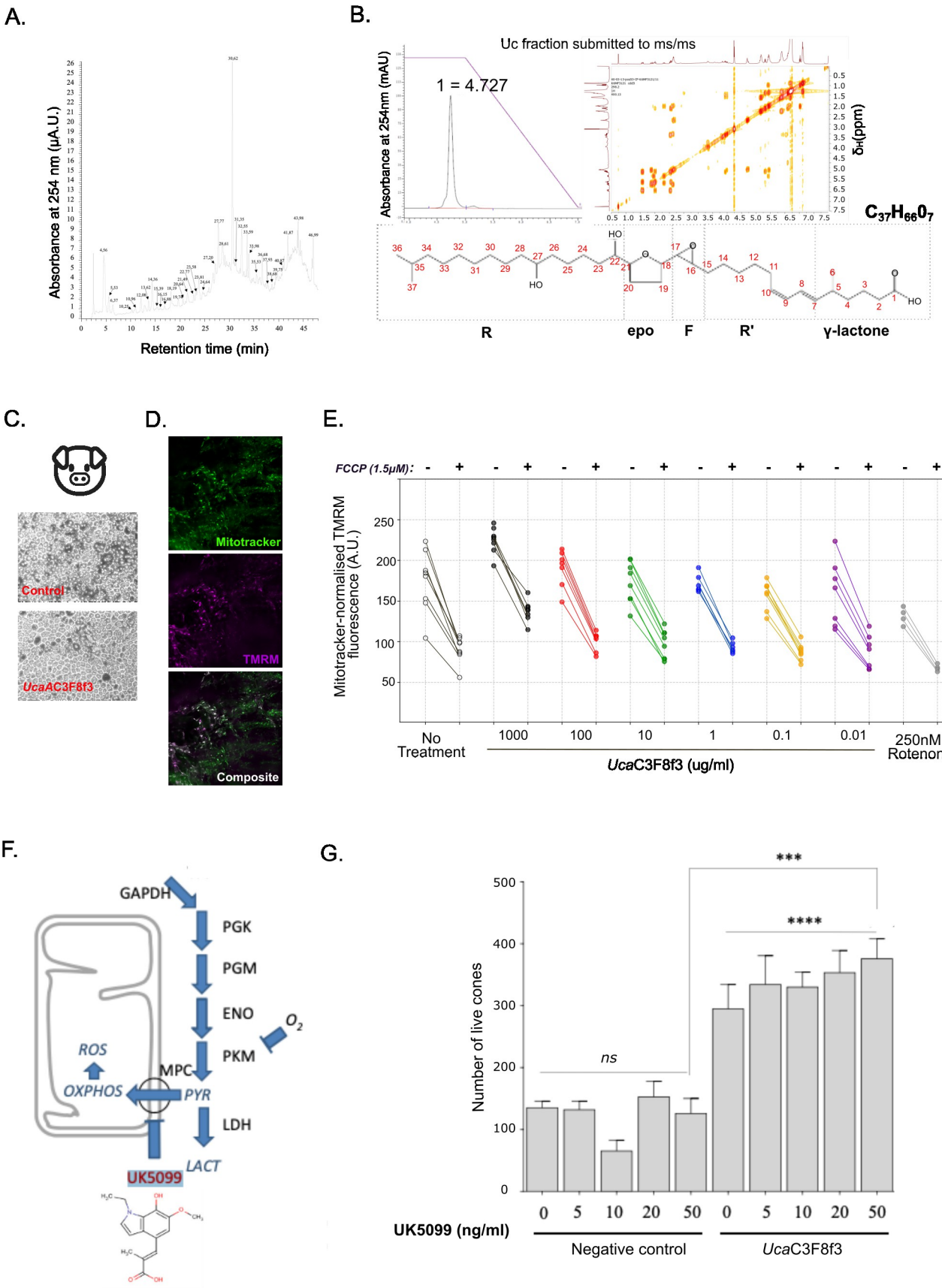

A.
Absorbance at 254 nm (µA.U.)
Retention time (min)
B.
Uc fraction submitted to ms/ms
Absorbance at 254nm (mAU)
1 = 4.727
δH(ppm)
C37H66O7
R
epo
F
R'
γ-lactone
C.
Control
UcaAC3F8f3
D.
Mitotracker
TMRM
Composite
E.
FCCP (1.5µM):
Mitotracker-normalised TMRM fluorescence (A.U.)
No Treatment
1000
100
10
1
0.1
0.01
250nM Rotenone
UcaC3F8f3 (ug/ml)
F.
GAPDH
PGK
PGM
ENO
O2
PKM
ROS
MPC
OXPHOS
PYR
LDH
LACT
UK5099
G.
***
****
ns
Number of live cones
UK5099 (ng/ml)
Negative control
UcaC3F8f3

Figure 4

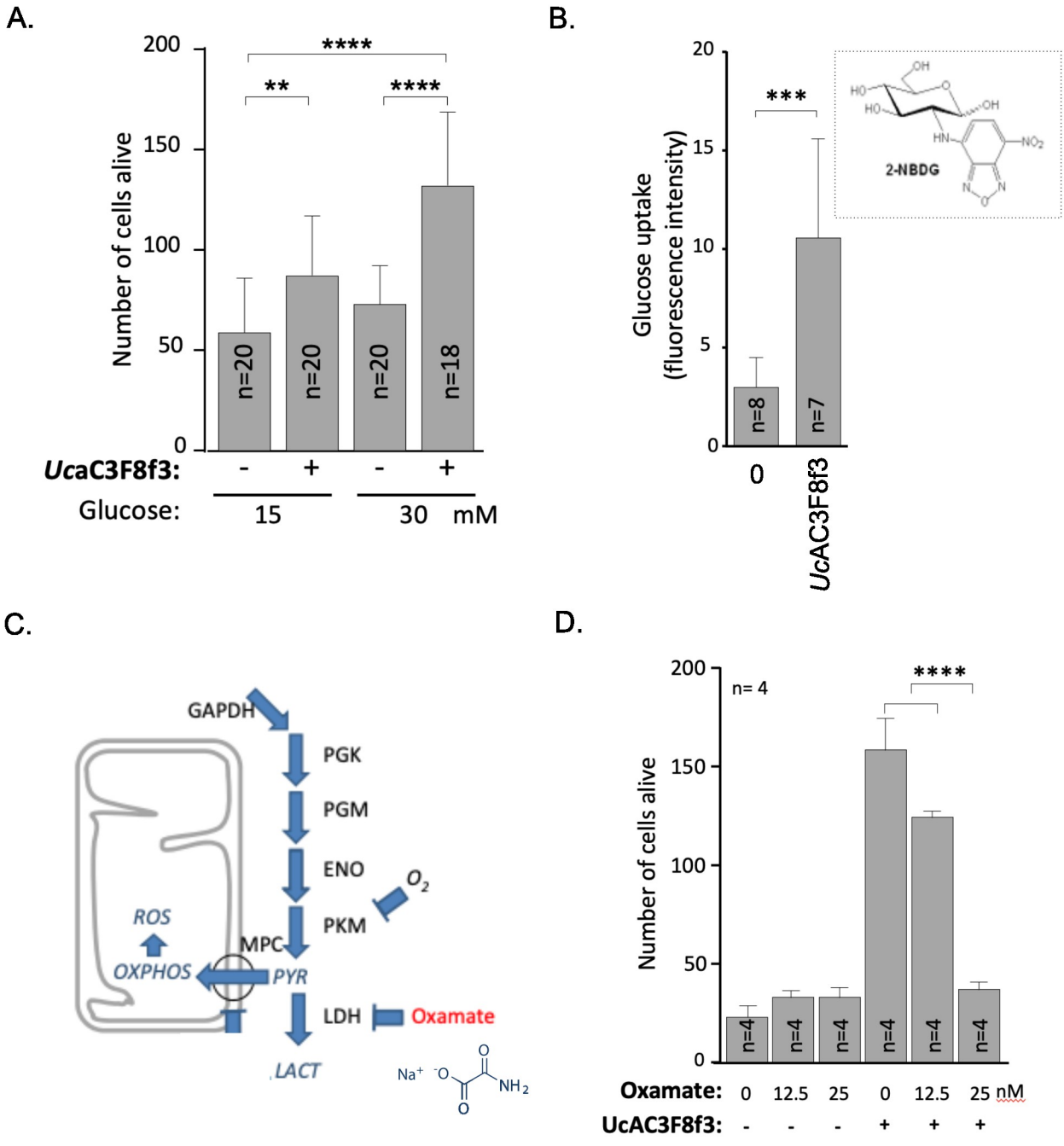

A.
Number of cells alive
200
150
100
50
0
****
**
****
n=20
n=20
n=20
n=18
UcaC3F8f3:
-
+
-
+
Glucose:
15
30
mM
B.
Glucose uptake
(fluorescence intensity)
20
15
10
5
0
***
n=8
n=7
0
UcAC3F8f3
2-NBDG
C.
GAPDH
PGK
PGM
ENO
PKM
O2
ROS
MPC
OXPHOS
PYR
LDH
Oxamate
LACT
Na+
NH2
D.
n= 4
****
Number of cells alive
200
150
100
50
0
n=4
n=4
n=4
n=4
n=4
n=4
Oxamate:
0
12.5
25
0
12.5
25
nM
UcAC3F8f3:
-
-
-
+
+
+

Figure 5

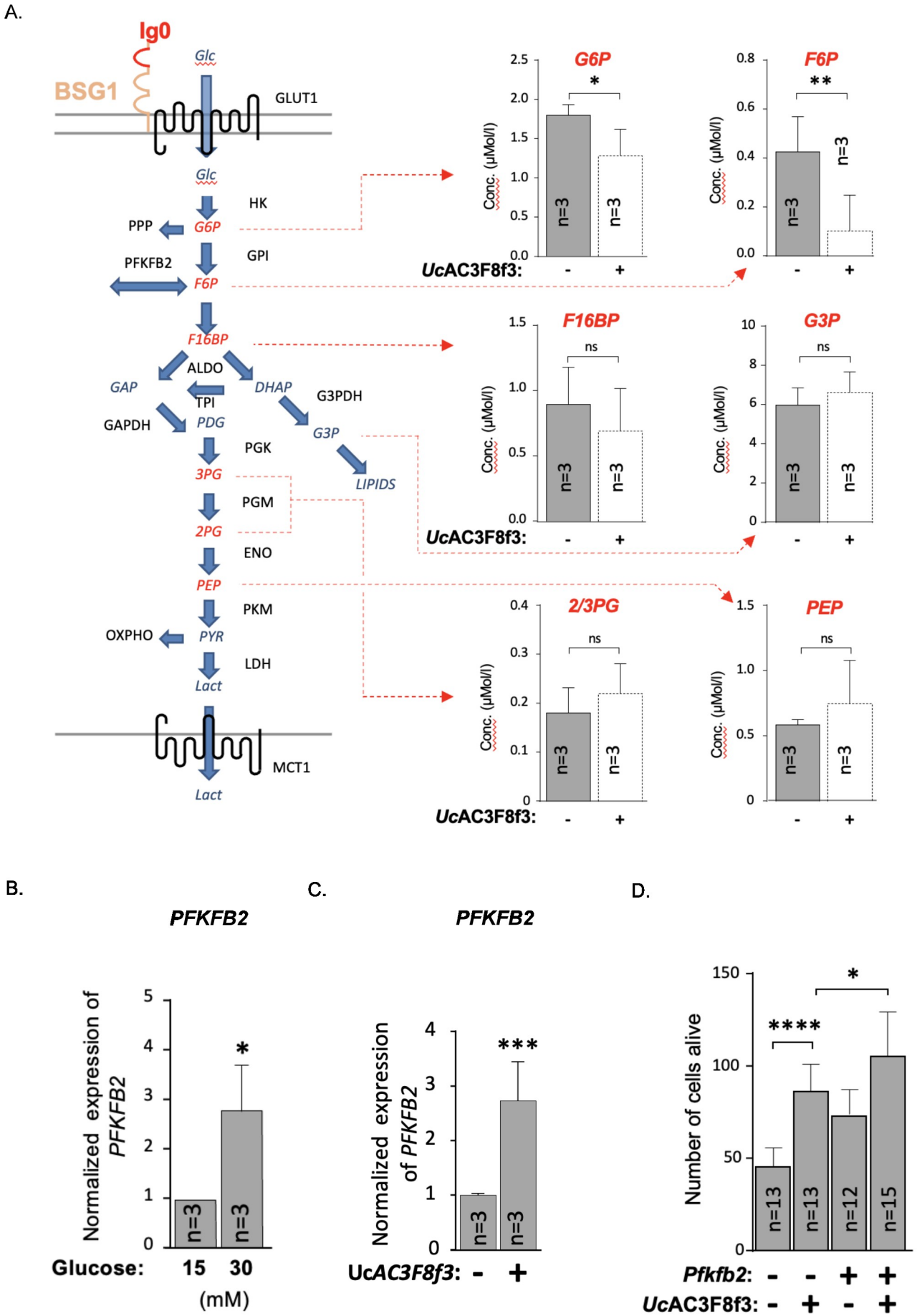
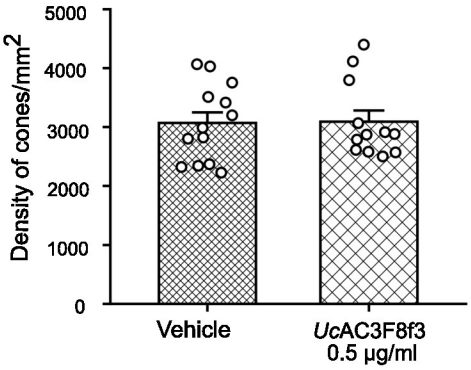

A.
Ig0
BSG1
Glc
GLUT1
Glc
HK
PPP
G6P
GPI
PFKFB2
F6P
F16BP
ALDO
GAP
DHAP
G3PDH
TPI
GAPDH
PDG
G3P
PGK
LIPIDS
3PG
PGM
2PG
ENO
PEP
PKM
OXPHO
PYR
LDH
Lact
MCT1
Lact
G6P
F6P
F16BP
G3P
2/3PG
PEP
Conc. (µMol/l)
n=3
ns
*
**
UcAC3F8f3: - +
B.
PFKFB2
Normalized expression of PFKFB2
Glucose: 15 30
(mM)
C.
PFKFB2
Normalized expression of PFKFB2
***
UcAC3F8f3: - +
D.
Number of cells alive
****
n=13
n=13
n=12
n=15
Pfkfb2: - - + +
UcAC3F8f3: - + - +

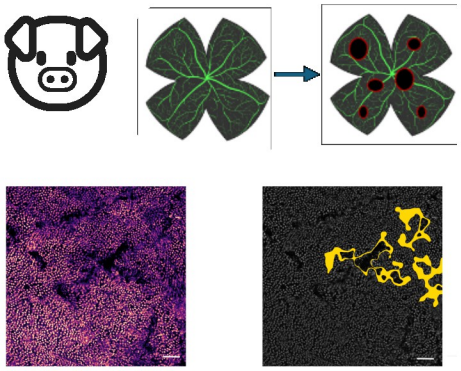
Figure 6

A.

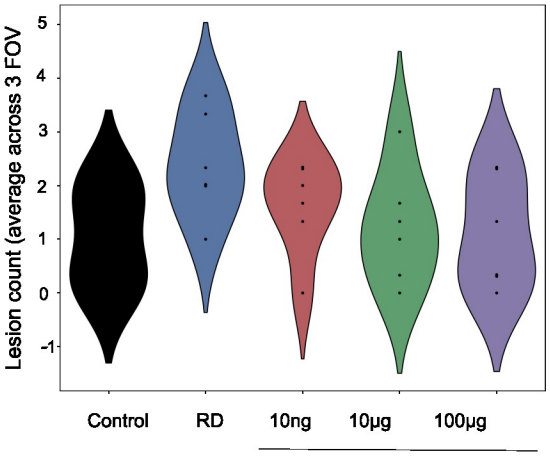




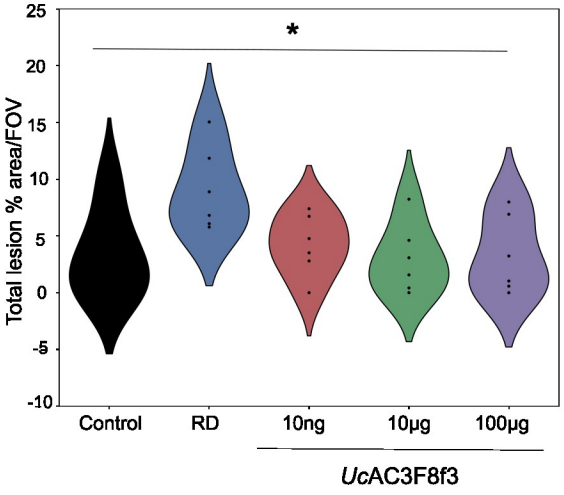
B.



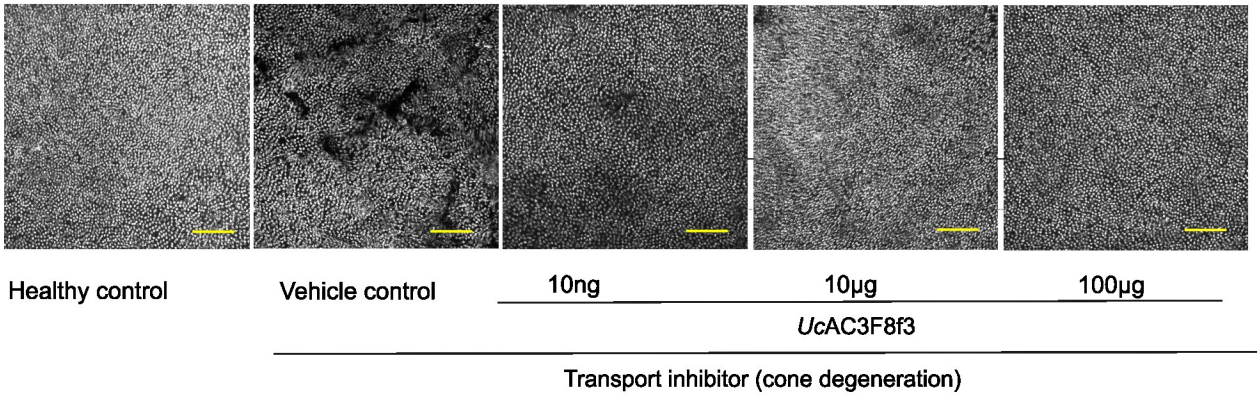
C.



D.



E.



Supplementary Files

This is a list of supplementary files associated with this preprint. Click to download.

- TableS1.pdf
- FigureS3.jpg
- FigureS2.jpg
- FigureS1.jpg